The 9th European Congress on Computational Methods in Applied Sciences and Engineering
ECCOMAS Congress 2024
3–7 June 2024, Lisboa, Portugal

EVALUATION OF MATERIAL MODELS USED IN MULTI-MATERIAL TOPOLOGY OPTIMIZATION

AHMED MOHAMED JUBARTALLA ALI[1,2], THÉODORE CHERRIÈRE[3], PETER GANGL[3], MARGIT GFÖHLER[2] AND MARIO KAPL[4]

[1] ADMiRE Research Center
Carinthia University of Applied Sciences
9524 Villach, Austria
e-mail: a.ali@fh-kaernten.at

[2] Faculty of Mechanical and Industrial Engineering
TU Wien
1040 Vienna, Austria

[3] Johann Radon Institute for Computational and Applied Mathematics (RICAM)
4040 Linz, Austria

[4] Department of Engineering & IT
Carinthia University of Applied Sciences
9524 Villach, Austria

Key words: Finite Element Method, Topology Optimization, Multi-Material, Material Model

Summary. We evaluate the behavior of several interpolations to perform density-based topology optimization among many lattice structures. The relevance of different non-standard mappings is compared to interpolating ten orthotropic microstructures with similar costs and densities. More precisely, the lattices (materials) are distributed in two different interpolation domains, namely, over the edges of a square domain and at the vertices of a non-orthogonal decagonal prism. In addition, the material properties are interpolated by using either a Lagrange polynomial, or Wachspress shape-functions. The performances are evaluated on a standard benchmark problem, i.e., the compliance minimization problem over an MBB beam. The results show that the use of an elaborated interpolation function or domain seems unnecessary for conducting multi-material topology optimization when using one family of micro-structures with similar geometric features.

1 INTRODUCTION

Since the early work of Bendsøe and Kikuchi [1], topology optimization has become a powerful design tool in mechanical engineering. Due to the high manufacturing flexibility offered by Additive Manufacturing, Multi-Material Topology Optimization (MMTO) of lattice structures has received considerable momentum in recent research. Several parameterizations are available in the literature when dealing with multiple discrete materials or composite orientations. Most of them are supported by several "density" fields $\rho_1, ..., \rho_n$ on a cartesian domain, $(\rho_1, ..., \rho_n) \in [0, 1]^n$ [2, 3, 4], or [5] more recently. It is also possible to interpolate the mate-

rial properties on non-orthogonal domains, such as convex polytopes [6]. These interpolations can be composed with additional penalization, such as the classical power law, so selecting the appropriate material mapping based on the number of used materials and evaluated properties (strength, stiffness, density, toughness, price, etc) could be challenging. This work aims to find a suitable model for optimizing lattices, including ten different micro-structures with similar costs and densities. In this study, we evaluate the performance of using combinations between two interpolation domains and two interpolation functions. The paper is organized as follows. Sec. 2 formulates the benchmark optimization problem. Then, Sec. 3 describes the candidate material mappings – interpolation domains and functions –, and the optimization results are analyzed in Sec. 4. Finally, Sec. 5 draws the conclusion and perspectives of this work.

2 FORMULATING THE OPTIMIZATION PROBLEM

This section introduces the discrete candidate materials and describes the associated two-scale topology optimization problem.

2.1 Candidate materials

In our previous work [7], three families of lattices containing superimposed parameterized X-shaped or XX-shaped lattices with square-shaped lattices were presented and used to optimize lattice structures. In this work, we restrict ourselves to one of these families (Fam #1) and treat its lattices as different candidate materials. Fig. 1 shows these lattices and their equivalent properties. At the end of the optimization, the algorithm should then converge to the materials; intermediate materials are not allowed due to manufacturability reasons.

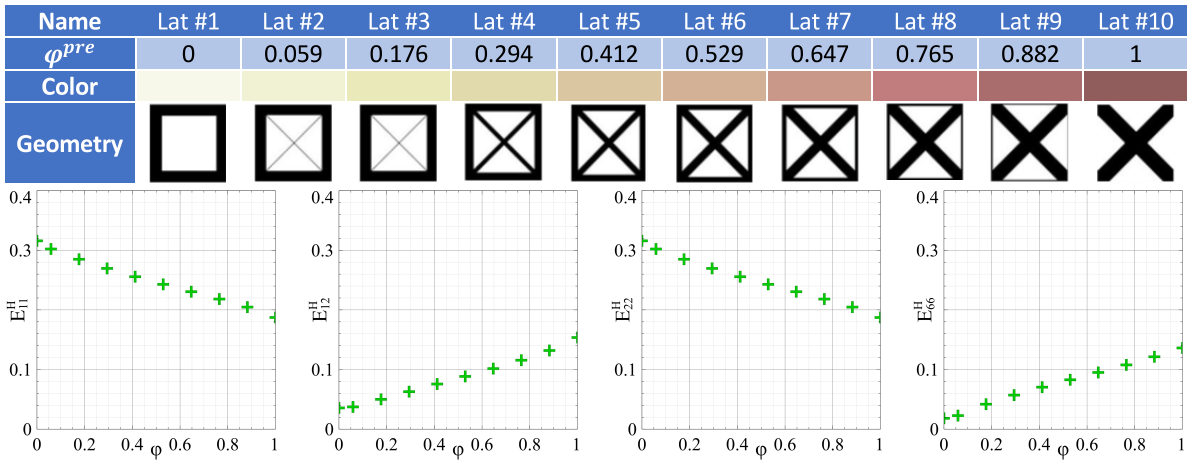

Figure 1: Micro-structures used in the study (top) and their effective elastic moduli (bottom)

2.2 Design variables

In order to apply an efficient gradient-based optimization algorithm, the material discreteness constraint is relaxed: therefore, the elastic moduli are interpolated by a differentiable mapping. For navigating between the materials, we use the following design variables per mesh element:

1. $\rho \in [0,1]$ distinguishes between void ($\rho = 0$) and solids ($\rho = 1$).
2. $\boldsymbol{\varphi}$ selects the lattice. This quantity can be a scalar, as in Fig. 1 where the ten lattices are associated with scalar predefined values φ^{pre}. It can also be a vector on non-standard interpolation domains, such as a regular decagon detailed in Sec. 3.

These design variables are optimized concurrently and can take any intermediate value during the optimization process. So, the elastic modulus $\mathbf{E}$ of an element n could be written as

$$\mathbf{E}_n(\rho_n, \boldsymbol{\varphi}_n) = E_n^{\text{den}}(\rho_n)\, \mathbf{E}_n^{\text{lat}}(\boldsymbol{\varphi}_n). \tag{1}$$

While the first part E_n^{den} is given by

$$E_n^{\text{den}} = E_{\min} + \rho_n^p (E_o - E_{\min}) \tag{2}$$

with a penalty factor p (in our case $p = 3$), the Young's modulus of the material E_o and a very small positive number $E_{\min}$ to prevent singularity (in our case $E_{\min} = 10^{-6}$), the second part $\mathbf{E}_n^{\text{lat}}$ depends only on the lattice and is interpolated in Sec. 3.2. After convergence, the resulting gray materials are projected to their nearest candidate lattices in φ^{pre}.

2.3 Optimization Problem

The problem is to minimize the compliance

$$C(\boldsymbol{\rho}, \boldsymbol{\varphi}) = \mathbf{U}^T(\boldsymbol{\rho}, \boldsymbol{\varphi})\, \mathbf{K}(\boldsymbol{\rho}, \boldsymbol{\varphi})\, \mathbf{U}(\boldsymbol{\rho}, \boldsymbol{\varphi}) \tag{3}$$

such that

$$\mathbf{K}(\boldsymbol{\rho}, \boldsymbol{\varphi})\ \mathbf{U}(\boldsymbol{\rho}, \boldsymbol{\varphi}) = \mathbf{F}, \tag{4}$$

$$G(\boldsymbol{\rho}) = \sum_{n=1}^{N} \rho_n - N \cdot V_f \leq 0, \tag{5}$$

and

$$0 \leq \rho_n \leq 1,$$
$$\boldsymbol{\varphi}_n \in \mathcal{D}_\varphi,$$

where $\mathbf{K}$, $\mathbf{U}$, and $\mathbf{F}$ are the stiffness matrix, displacement vector, and load vector, respectively; V_f is the allowed volume fraction; and $\mathcal{D}_\varphi$ is an interpolation domain associated with $\boldsymbol{\varphi}$ detailed in Sec. 3. The sensitivities are calculated from Eq. 3, 4, and 5 and according to Eq. 1 as

$$\begin{aligned}
\frac{\partial C}{\partial \rho_n} &= -\frac{\partial E_n^{\text{den}}}{\partial \rho_n} \mathbf{u}_n^T \left(\int_{\Omega_n} \mathbf{B}^T \mathbf{E}_n^{\text{lat}} \mathbf{B} \mathrm{d}\Omega_{\mathrm{n}} \right) \mathbf{u}_n, \\
\frac{\partial C}{\partial \varphi_n} &= -E_n^{\text{den}} \mathbf{u}_n^T \left(\int_{\Omega_n} \mathbf{B}^T \frac{\partial E_n^{\text{lat}}}{\partial \varphi_n} \mathbf{B} \mathrm{d}\Omega_{\mathrm{n}} \right) \mathbf{u}_n, \\
\frac{\partial G(\rho)}{\partial \rho_n} &= 1,
\end{aligned}$$

where Ω_n is the mesh domain of element n, $\mathbf{B}$ is the strain-displacement matrix, $\partial E_n^{\text{den}}/\partial \rho_n$ is obtained from Eq. 2, and $\partial \mathbf{E}_n^{\text{lat}}/\partial \varphi_n$ is obtained from Eq. 7, 8, or 9, depending on the selected interpolation function. In order to prevent checker-board effect, we modify the term $\partial E_n^{\text{den}}/\partial \rho_n$ using the sensitivity filter [8] with a radius of $R_{\min} = 2.0$ mesh elements.

3 MATERIAL MODELS

To study the effect of the material interpolation, we evaluate two interpolation domains as well as two interpolation functions.

3.1 Interpolation domains

We compare two interpolation domains: a *square* domain and a *decagonal prism*. The former is $2D$ and orthogonal, while the latter is $3D$ and non-orthogonal.

3.1.1 Square domain

This is the most simple domain used in $2D$, where $\mathcal{D}_\varphi = [0, 1]$. We divide the vertical edges of the domain into nine segments. Void is assigned to all the left nodes, while the lattices are distributed over the right ones according to their φ^{pre} values, as depicted in Fig. 2a. An advantage of such an orthogonal domain is that the strayed points are easy to handle by the following projection

$$\text{Proj}(\varphi_n) = \min(\max(\varphi_n, 0), 1). \tag{6}$$

3.1.2 Decagonal prism

Orthogonal domains are not suitable for all optimization problems. An example is given in [6]: the conductors of an electrical machine are of the same nature, so they should be placed on the same plane according to their discrete electrical phase. This consideration leads to a diamond-shaped domain where the bottom is void, the midplane includes the conductors, and the top is iron. Since this work also considers discrete materials of the same nature, it might make sense to follow the same idea by defining the interpolation domain $\mathcal{D}$ as a regular decagon, which includes the ten lattices, and extruding it to the void along the ρ-axis. Then, we assign voids to the front face ($\rho = 0$) and place the materials at the vertices of the back side ($\rho = 1$), in a symmetric order as shown in Fig. 2b. The order of the lattices is chosen to avoid the jump in the properties between each of the two adjacent ones.

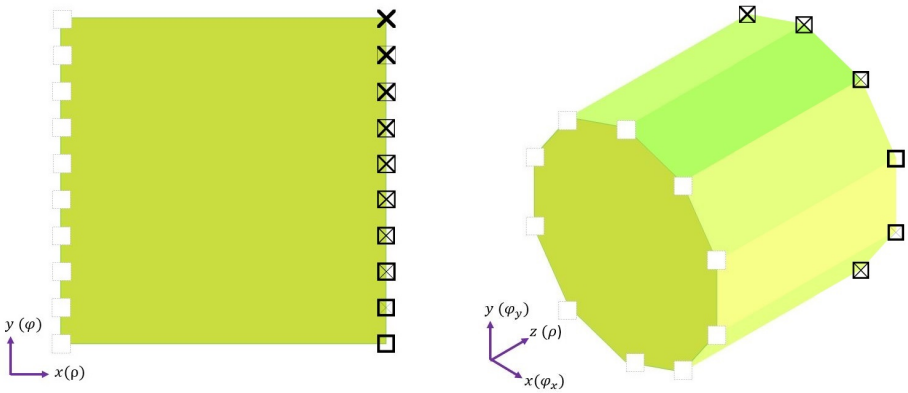

(a) Square domain (b) Decagonal domain

Figure 2: Interpolation domains

The coordinates of a specific vertex (m) is obtained by using:

$$x_m = \frac{1}{2}\cos(\phi_m) + \frac{1}{2},$$
$$y_m = \frac{1}{2}\sin(\phi_m) + \frac{1}{2},$$

where the angle ϕ is also given in Tab. 1. In this domain, the variable $\boldsymbol{\varphi}$ is a 2D vector describing the position in the decagon and, therefore, selecting the lattice.

Table 1: Angles and assigned materials for the vertices of the decagonal prism

Vertex	Angle ϕ	Material
1	$\frac{1}{5}\pi$	Lat #1
2	$\frac{2}{5}\pi$	Lat #3
3	$\frac{3}{5}\pi$	Lat #5
4	$\frac{4}{5}\pi$	Lat #7
5	$\frac{5}{5}\pi$	Lat #9
6	$\frac{6}{5}\pi$	Lat #10
7	$\frac{7}{5}\pi$	Lat #8
8	$\frac{8}{5}\pi$	Lat #6
9	$\frac{9}{5}\pi$	Lat #4
10	$\frac{10}{5}\pi$	Lat #2

3.2 Interpolation functions

Similar to the previous subsection, we evaluate two approaches for interpolating the second part of Eq. 1, i.e. $\mathbf{E}_n^{\text{lat}}$. More precisely, we employ Lagrange and Wachspress interpolations.

3.2.1 Lagrange interpolation

This method could be combined in almost all domains. We interpolate the elastic modulus for the square, where φ_n is a scalar, as

$$\mathbf{E}_n^{\text{lat}} = \sum_{i=0}^{q} \mathbf{A}_i \cdot (\varphi_n)^i, \tag{7}$$

and for the prism, where $\boldsymbol{\varphi}_n = (\varphi_n^x, \varphi_n^y)$ is a 2D vector, as

$$\mathbf{E}_n^{\text{lat}} = \sum_{j=0}^{q_{\text{x}}} \sum_{k=0}^{q_{\text{y}}} \mathbf{B}_{jk} \cdot (\varphi_n^{\text{x}})^j \cdot (\varphi_n^{\text{y}})^k, \tag{8}$$

respectively, where q, q_{x}, and q_{y} are the fitting degrees (in our case $q = q_{\text{x}} = q_{\text{y}} = 3$ gives satisfactory precision) and $\mathbf{A}_i$ and $\mathbf{B}_{jk}$ are matrices of fitting coefficients.

3.2.2 Wachspress interpolation

This interpolation comes from a generalization of barycentric coordinates used in the finite element method [9] and is compatible with strictly convex polytopes. Accordingly, we combine it with the decagonal prism. The elastic modulus of an element n is interpolated regarding its location inside the domain as

$$\mathbf{E}_n^{\text{lat}} = \sum_{m=1}^{M} \omega_m(\boldsymbol{\varphi}_n) \cdot \mathbf{E}_m \tag{9}$$

with

$$\begin{aligned} \omega_m(\boldsymbol{\varphi}_n) &= \frac{\phi_m(\boldsymbol{\varphi}_n)}{\sum_{i=1}^{M} \phi_i(\boldsymbol{\varphi}_n)}, \\ \phi_m(\boldsymbol{\varphi}_n) &= \frac{A_m}{A_m^+(\boldsymbol{\varphi}_n) \cdot A_m^-(\boldsymbol{\varphi}_n)}, \end{aligned}$$

where $A_m^+(\boldsymbol{\varphi}_n)$, $A_m^-(\boldsymbol{\varphi}_n)$, and A_m are the (signed) areas of the triangles shown in Fig. 3 for a simpler pentagonal domain, cf. [10]. Compared with the previous square domain, it is more involved in handling constraints in a non-orthogonal domain; there is no simple formula such as (6). For simplicity, we use a radial projection of the points outside the decagon shown in Fig. 3, applied after each update of the optimization variable $\boldsymbol{\varphi}$.

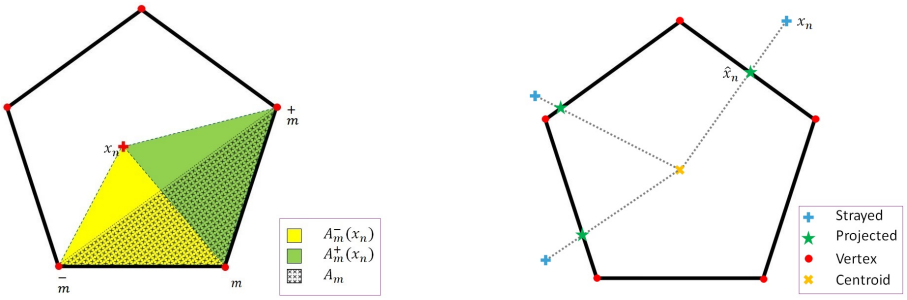

Figure 3: Illustration of the Wachspress coordinates (left) and projection of the strayed points (right) for a pentagonal domain

4 RESULTS

In this section, we solve an MBB beam problem as a benchmark to assess the different combinations of interpolation domains and functions introduced in the previous section.

A schematic of our MBB beam problem is given in Fig. 4. The beam has a length and height of 1.00 and 0.25, respectively, and holds a pressure of 1.00 distributed over a strip of 0.10. Due to its symmetry, we only discretize the right half using 50×25 plane-strain elements and set the volume fraction to $V_{\text{f}} = 40\%$.

Using Wachspress interpolation is not directly possible for the square domain because not all materials are placed over vertices; see Fig 2a. Accordingly, we combine it with Lagrange interpolation. In contrast, the decagonal domain is compatible with both types of interpolations.

Then, we solve the problem using the Method of Moving Asymptotes (MMA) [11]. Fig. 5 shows the optimization histories for the objective function and volume constraint. Typical

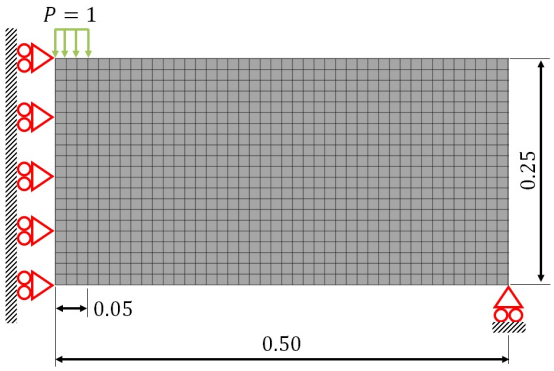

Figure 4: Schematic for the MBB beam problem

behaviors are seen in the two sub-figures, where the objective value drops steeply at the beginning of the process and then reduces slowly until convergence. The volume constraint similarly fluctuates around V_f value but then stabilizes. It is worth mentioning that the objective values do not represent the structural compliance due to the fact that the design variables are relaxed. For obtaining the physical compliance (Tab. 2), the values of $\boldsymbol{\varphi}_n$ need to be projected to their nearest φ^{pre}.

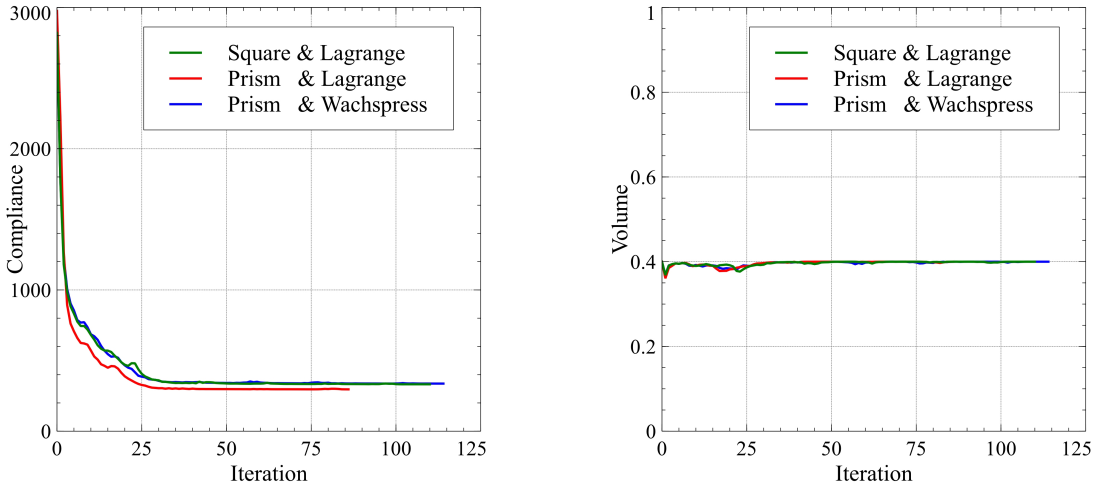

Figure 5: Optimization histories for the compliance and volume constrain

Fig. 6 shows the optimized designs: the optimized values of $\boldsymbol{\rho}$ are plotted in the upper subplots, while the optimized values of the lattices $\boldsymbol{\varphi}$ are displayed in the lower subplots. Generally, the three models converged to similar designs. All the designs have uniform distributions and transitions between the lattices with very few isolated elements. On the one hand, light brown (square) micro-structures are seen at the upper and lower regions due to their directional strength, as expected. On the other hand, the dark (cross) microstructures, with their high shear strength, fill the region between them.

Since the prism domain has more dimensions than the square, it should offer more connections between lattices and more freedom to the optimization algorithm; it is, therefore, expected to

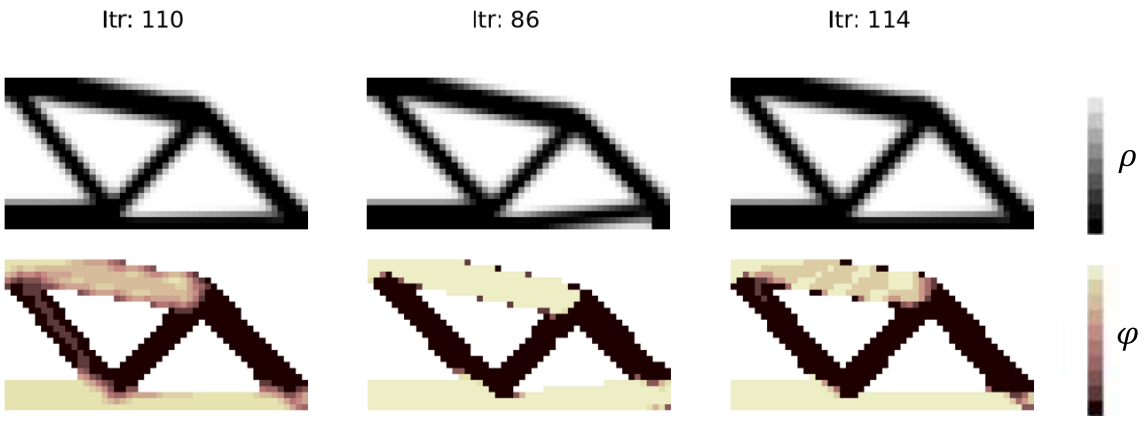

(a) Square & Lagrange (b) Prism & Lagrange (c) Prism & Wachspress

Figure 6: Optimized designs obtained with different interpolation domains and functions

converge to a better optimum. However, when comparing the numbers in Tab. 2, it is found that compliance is lower when using the square domain. The interpolation function also plays a role: Wachspress interpolation leads to comparable results with the prism domain, while the Lagrange interpolation seems to return a different and worse local optimum.

Table 2: Optimized compliance for the studied interpolation domains and functions

Interpolation Domain	Interpolation Function	
	Lagrange	Wachspress
Square	331.79	N/A
Decagonal	368.28	334.94

In addition, when comparing the computational costs, using non-orthogonal domains requires a potentially time-consuming treatment of the strayed design points. One of the simplest methods is to project them back onto the polygon. Different types of projection may be used, such as the radial projection (see Fig. 3, right) or minimal distance (orthogonal) projection. However, this has to be done individually for each mesh element, which requires additional cost, especially in $3D$ and higher dimensional domains. Therefore, it is preferable to keep an orthogonal domain in our case, where only two types of micro-structures are mixed together.

5 CONCLUSION

In this paper, we studied different multimaterial interpolation schemes in which the number of design variables does not depend on the number of candidate materials. We solved an MBB beam optimization problem to compare the behaviors of material models combined from the square domain and decagonal prism domain on the one hand and Lagrange polynomial and Wachspress interpolations on the other hand. The results showed that using the simplest scheme consisting

of a square domain with Lagrange interpolation would result in better-optimized designs and lower computational cost than if the materials were wisely arranged within a higher dimensional domain. However, this might not be the case anymore when additional families of lattices are included in the optimization, which will be addressed in future work.

ACKNOWLEDGEMENT

The research presented in this paper has been supported by the Federal Ministry for Digital and Economic Affairs (BMDW) within the framework of COIN "Aufbau", 8th call of the Austrian Research Promotion Agency (FFG) – project number 884136 (iLEAD).

REFERENCES

[1] M. P. Bendsøe and N. Kikuchi, "Generating optimal topologies in structural design using a homogenization method," *Computer Methods in Applied Mechanics and Engineering*, vol. 71, p. 197–224, Nov. 1988.

[2] J. Stegmann and E. Lund, "Discrete material optimization of general composite shell structures," *International Journal for Numerical Methods in Engineering*, vol. 62, p. 2009–2027, Feb. 2005.

[3] M. Bruyneel, "SFP-a new parameterization based on shape functions for optimal material selection: Application to conventional composite plies," *Structural and Multidisciplinary Optimization*, vol. 43, no. 1, pp. 17–27, 2011.

[4] T. Gao, W. Zhang, and P. Duysinx, "A bi-value coding parameterization scheme for the discrete optimal orientation design of the composite laminate," *International Journal for Numerical Methods in Engineering*, vol. 91, p. 98–114, May 2012.

[5] B. Yi, G. H. Yoon, R. Zheng, L. Liu, D. Li, and X. Peng, "A unified material interpolation for topology optimization of multi-materials," *Computers & Structures*, vol. 282, p. 107041, July 2023.

[6] T. Cherrière, L. Laurent, S. Hlioui, F. Louf, P. Duysinx, C. Geuzaine, H. Ben Ahmed, M. Gabsi, and E. Fernández, "Multi-material topology optimization using wachspress interpolations for designing a 3-phase electrical machine stator," *Structural and Multidisciplinary Optimization*, vol. 65, Nov. 2022.

[7] A. M. J. Ali, L.-M. Faller, M. Gföhler, F. O. Riemelmoser, and M. Kapl, "A two-scale topology optimization method for functionally graded lattice structures using three families of micro-structures," *Computer-Aided Design & Applications*, vol. 21, no. 2, pp. 179–198, 2024.

[8] O. Sigmund, "On the design of compliant mechanisms using topology optimization," *Mechanics of Structures and Machines*, vol. 25, no. 4, pp. 493–524, 1997.

[9] E. L. Wachspress, *A Rational Finite Element Basis*. Elsevier, 1975.

[10] T. Cherrière and L. Laurent, "tcherrie/wachspress2d3d," Mar. 2023. `https://doi.org/10.5281/zenodo.7701776`.

[11] A. Deetman, "Python code of the method of moving asymptotes," 2019. `https://github.com/arjendeetman/GCMMA-MMA-Python`.